Hydrodynamic Forces on Spillway Torque-Tube Gates

Luis A. de Béjar, M.ASCE[1]; and Richard L. Stockstill, F.ASCE[2]

Abstract: The critical hydraulic configuration for a set of torque-tube gates controlling the flow through the navigable portion of a spillway was experimentally identified. In this paper, an analytical model for the upstream pressure field on a typical gate within the set is constructed. The gate rotation from the maximum elevation (gate in closed position) and the hydraulic torque transmitted by the pressure field to the gate tube are formulated. Mean values of parameters of response are often sufficient for the preliminary design of a gate. The dispersions of these parameters of response, which are necessary for the final design of a gate, may be computed using the corresponding mean-square values. These were obtained empirically in a flume from experiments on a 1/15-scale physical model of a set of three prototype gates for the Montgomery Point Lock and Dam project. Theoretical predictions of parameter mean and mean-square values compare well with the average corresponding statistics obtained experimentally.

DOI: 10.1061/(ASCE)HY.1943-7900.0000216

CE Database subject headings: Hydraulic pressure; Hydraulic structures; Spillways; Gates; Hydrodynamics.

Author keywords: Hydraulic forces; Hydraulic pressure field; Hydraulic physical models; Hydraulic structures; Navigable spillways; Torque-tube gates.

Introduction

The flow through the navigable portion of a river barrier may be conveniently controlled by a parallel array of torque-tube gates, as Fig. 1 illustrates (see, for example, Fletcher and de Béjar 1995 for a detailed description of the hydraulic structural 10-gate scheme in the Montgomery Point Lock and Dam project).

The torque-tube type of flap gate is operated by controlling the magnitude of the torsional moment applied to the structural tube rigidly connected to the gate panel at its lower horizontal edge (Sehgal et al. 1997). Fig. 2(a) shows a typical torque-tube gate for flow control in navigational spillways. In the case of the Montgomery Point Lock and Dam project, the generally curved gate skin adopts a circular profile, and the gate elevation is identified by the angle that the tangent to the skin circle makes with the horizontal plane at the connection to the tube. The gates operate at an elevation ranging from zero (an open, horizontal, position) to 70° in the closed-gate condition.

Each possible combination of individual operational gate elevations within a given gate set is subjected to complex hydraulic loading, and the task of identifying the critical gate configuration governing the hydraulic structural design necessarily involves the application of both analytical and experimental techniques.

Investigations during the past two decades have directed attention to experimental analysis (Naudascher 1991; Naudascher and Rockwell 1994) and to updating design guidelines of spillway gates (Sehgal 1996; Sagar 1995). In particular, Sehgal (1996) and Viparro and Hansen (1993) discussed general features of the torque-tube type of flap gate, but due to the complexity of hydraulic conditions, recommendations regarding design loads are limited. This paper presents experimentally verified mathematical models that address this need for the case of navigable spillway torque-tube gates.

An analytical description of the pressure distribution on the upstream face of a typical gate in the critical configuration is derived, and the associated torque transmitted to the gate tube is computed [Fig. 2(b)]. The theoretical pressures and torque are compared to the laboratory data from experiments on a carefully instrumented 1/15-scale physical model of a prototype Montgomery Point gate at the U.S. Army Engineer Research and Development Center, and the second-moment characterization of the tube's torque response to the imposed loads is verified.

During the experiments, it was recognized that the largest hydraulic forces acting on a single central gate occur when all gates in the experimental flume simultaneously face the flow in a fully closed position (de Béjar 1995). Fig. 3 illustrates this critical configuration. This figure shows the basic depths recorded in the flow overpassing the system of gates: the depth of the nappe at the gate crest (h_f=59 mm), the smallest depth in the free-falling cascade (33 mm), and the depth of the enclosed tailwater pool (128 mm). For the purpose of evaluating design hydraulic forces on the gate with a ventilated nappe, it is conservative to ignore the hydrostatic pressure field on the back of the gate. This tailwater pressure was verified as minor for other gate configurations in the experiments, as, for example, when the central gate in a set of three is fully closed and the adjacent lateral gates are in a full open position, or when only the central gate in a set of three is fully open and the adjacent lateral gates are in a full closed position.

At the outset, some limitations of the mathematical models to be developed are noted: (1) The change in the flow pressure field due to the gate vibrations is neglected and (2) the models accu-

[1]Research Structural Engineer, U.S. Army Engineer Research & Development Center (ERDC), Vicksburg, MS 39180-6199 (corresponding author). E-mail: Luis.A.DeBejar@erdc.usace.army.mil

[2]Research Hydraulic Engineer, U.S. Army Engineer Research & Development Center (ERDC), Vicksburg, MS 39180-6199. E-mail: Richard.L.Stockstill@erdc.usace.army.mil

Note. This manuscript was submitted on April 15, 2009; approved on February 26, 2010; published online on March 4, 2010. Discussion period open until March 1, 2011; separate discussions must be submitted for individual papers. This paper is part of the ***Journal of Hydraulic Engineering***, Vol. 136, No. 10, October 1, 2010. ©ASCE, ISSN 0733-9429/2010/10-681–692/$25.00.

Report Documentation Page

Form Approved
OMB No. 0704-0188

1. REPORT DATE	2. REPORT TYPE	3. DATES COVERED
OCT 2010		**00-00-2010 to 00-00-2010**

4. TITLE AND SUBTITLE	5a. CONTRACT NUMBER
Hydrodynamic Forces On Spillway Torque-Tube Gates	5b. GRANT NUMBER
	5c. PROGRAM ELEMENT NUMBER
6. AUTHOR(S)	5d. PROJECT NUMBER
	5e. TASK NUMBER
	5f. WORK UNIT NUMBER
7. PERFORMING ORGANIZATION NAME(S) AND ADDRESS(ES) **U.S. Army Engineer Research & Development Center (ERDC),Research Structural Engineer,Vicksburg,MS,39180**	8. PERFORMING ORGANIZATION REPORT NUMBER
9. SPONSORING/MONITORING AGENCY NAME(S) AND ADDRESS(ES)	10. SPONSOR/MONITOR'S ACRONYM(S)
	11. SPONSOR/MONITOR'S REPORT NUMBER(S)

12. DISTRIBUTION/AVAILABILITY STATEMENT
Approved for public release; distribution unlimited

13. SUPPLEMENTARY NOTES
Journal of Engineering Mechanics, October 2010, pgs 681-692

14. ABSTRACT
The critical hydraulic configuration for a set of torque-tube gates controlling the flow through the navigable portion of a spillway was experimentally identified. In this paper, an analytical model for the upstream pressure field on a typical gate within the set is constructed. The gate rotation from the maximum elevation gate in closed position and the hydraulic torque transmitted by the pressure field to the gate tube are formulated. Mean values of parameters of response are often sufficient for the preliminary design of a gate. The dispersions of these parameters of response, which are necessary for the final design of a gate, may be computed using the corresponding mean-square values. These were obtained empirically in a flume from experiments on a 1/15-scale physical model of a set of three prototype gates for the Montgomery Point Lock and Dam project. Theoretical predictions of parameter mean and mean-square values compare well with the average corresponding statistics obtained experimentally.

15. SUBJECT TERMS

16. SECURITY CLASSIFICATION OF:			17. LIMITATION OF ABSTRACT	18. NUMBER OF PAGES	19a. NAME OF RESPONSIBLE PERSON
a. REPORT **unclassified**	b. ABSTRACT **unclassified**	c. THIS PAGE **unclassified**	**Same as Report (SAR)**	**12**	

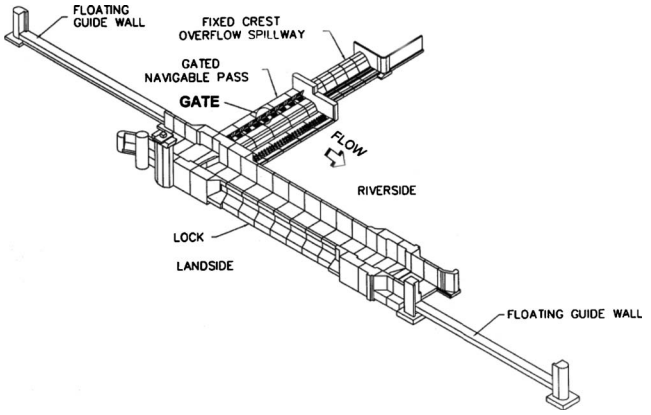

Fig. 1. Montgomery Point Lock and Dam: application of torque-tube gates for flow control in a navigable spillway

rately represent the behavior of the set of gates in a uniformly closed position (70° elevation) only if the back of the gates is ventilated. For unventilated gates, strong turbulence may form against their backs, thus invalidating the underlying assumptions.

Hydraulic Pressure Field

To construct a mathematical model, the following simplifying assumptions are postulated. Water is assumed an incompressible, inviscid, and homogeneous fluid, and its flow is taken as irrotational. The critical hydrostructural configuration is considered, i.e., the upstream flow at its maximum operational headwater pool running over the torque-tube gate in a closed position.

Consider the idealized unit-width control volume $D'DA^{iv}ABB'A''A'''D'$ in Fig. 2(b) and its natural partition into two subvolumes by the vertical plane $A'''A^{iv}$. For simplicity, the flow was assumed to enter and exit the volume with uniform velocities U and u, respectively. However, this assumption for the exit velocity u is probably unconservative since a slightly inclined velocity vector generally produces a larger resisting moment at the gate tube. The forces acting on the boundary surface are schematically represented in the diagram. The weights of water in the various parts of the control volume are designated by W_i, $i=1$, 2, and 3. The vertical and horizontal components of the force exerted by the gate on the flow act at point Q and are denoted by R_1 and R_2, with lever arms r_1 and r_2, respectively, about the pivoting point A.

Assuming that the flow through AA'' is approximately horizontal, the vertical equilibrium of control volume $ABB'A''A$ may be expressed as (Prandtl and Tietjens 1957; Shames 1995)

$$R_1 - W_2 - W_3 = 0 \tag{1}$$

Notice that the discontinuity $A''A'''$ in this geometric simplification also introduces some error. In reality, the flow free surface provides a smooth transition from line $D'A'''$ to line $A''B'$, as indicated schematically by the dotted curve in Fig. 2(b). Therefore, in reality, there is a small additional water weight acting on $A''B'$ that is neglected in the geometric idealization.

In the absence of horizontal body forces, the equation of conservation of linear momentum applied to the whole control volume in Fig. 2(b) may be expressed as

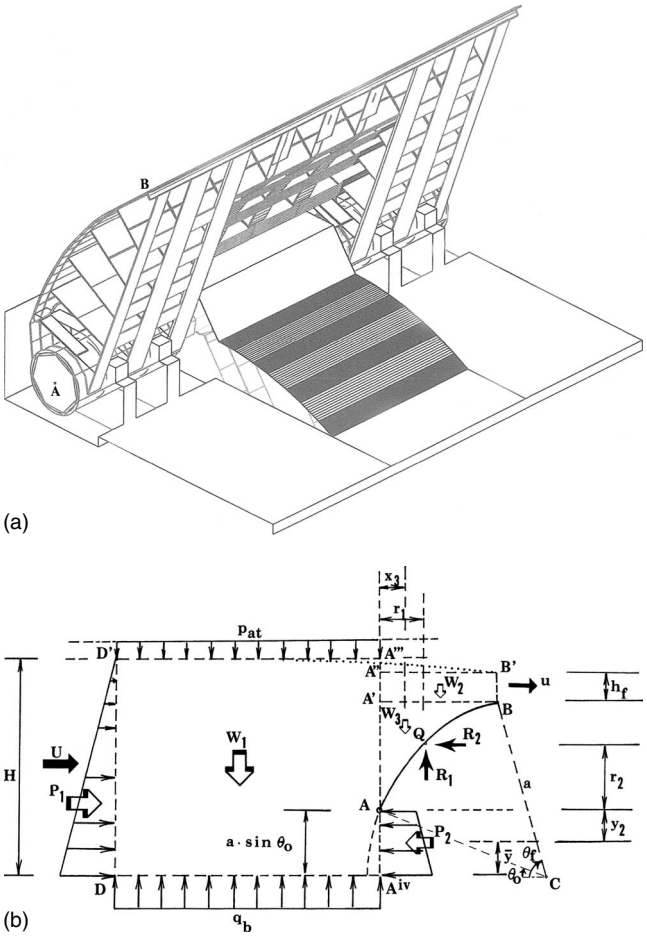

Fig. 2. (a) Typical torque-tube gate; (b) idealized control volume

$$P_1 - P_2 - R_2 = -U^2 \rho A_D + u^2 \rho A_B \tag{2}$$

where P_1 and P_2=resultant forces of pressures acting on sides DD' and AA^{iv} of the control volume, respectively; A_D and A_B =cross-sectional areas of the control volume at Locations D and B, respectively; U and u=corresponding flow velocities, assumed

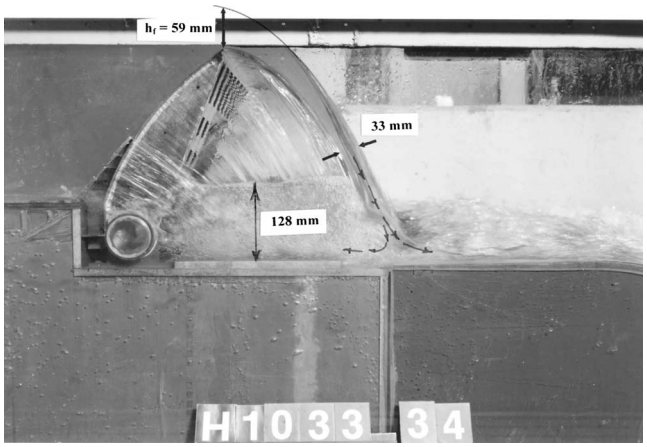

Fig. 3. Physical model of Montgomery Point torque-tube gate. Design controlling condition: lateral view of three gates in the experimental flume in closed position

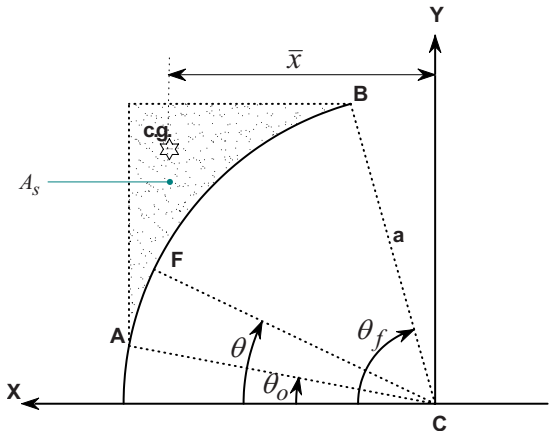

Fig. 4. Area subtended by gate arc AB (shaded)

to have a direction normal to the respective cross-sectional areas; and ρ=mass density of water.

Notice that the assumption of a zero hydrostatic pressure on the segment BB' implies that this segment is taken a short distance into the free jet. The approximation of a zero gauge-pressure free jet is adequate for small values of h_f (Street et al. 1996).

The theorem of moment of momentum about point A, applied to the whole control volume, produces the following equation:

$$P_1\left(\frac{H}{3} - a\sin\theta_0\right) + W_2\frac{a}{2}(\cos\theta_0 - \cos\theta_f) + W_3 \cdot x_3 + P_2 \cdot y_2 - R_1 \cdot r_1 - R_2 \cdot r_2 = -\left(\frac{H}{2} - a\sin\theta_0\right)U^2\rho A_D + \left[a(\sin\theta_f - \sin\theta_0) + \frac{h_f}{2}\right]u^2\rho A_B \tag{3}$$

where H and h_f=approach depth and the brink depth, respectively; θ_0 and θ_f=elevation angles of points A and B, which are the respective ends of the circular gate AB in closed position; and a=gate radius.

Since point Q is on the circle, the following relationship is satisfied

$$(a\cos\theta_0 - r_1)^2 + (a\sin\theta_0 + r_2)^2 = a^2 \tag{4}$$

Next, consider the generating radius vector with center at C, magnitude a, and argument $\theta \in (\theta_0, \theta_f)$, shown in Fig. 4. The shaded area A_s is given by

$$A_s = \int_{a\cos\theta_f}^{a\cos\theta_0}\int_{\sqrt{a^2-x^2}}^{a\sin\theta_f} dydx = a^2\left[\sin\theta_f(\cos\theta_0 - \cos\theta_f) + \frac{1}{4}(\sin 2\theta_f - \sin 2\theta_0) - \left(\frac{\theta_f - \theta_0}{2}\right)\right] \tag{5a}$$

and its centroidal point has abscissa

$$\bar{x} = \frac{1}{A_s}\int_{a\sin\theta_0}^{a\sin\theta_f}\int_{\sqrt{a^2-y^2}}^{a\cos\theta_0} xdxdy = \frac{1}{2A_s}\left[\frac{a^3}{3}(\sin^3\theta_f - \sin^3\theta_0) - a^3\sin^2\theta_0(\sin\theta_f - \sin\theta_0)\right] \tag{5b}$$

The weight of water corresponding to the area A_s is $W_3=\gamma\cdot A_s$, where $\gamma=\rho\cdot g$=the unit weight of water and g= acceleration of gravity. The line of action of W_3 is defined by

$$x_3 = a\cos\theta_0 - \bar{x} \tag{5c}$$

Now, the reactive force R_1 may be computed from Eq. (1) as

$$R_1 = W_2 + W_3 = \gamma \cdot a \cdot h_f \cdot (\cos\theta_0 - \cos\theta_f) + W_3 \tag{6}$$

in which the brink depth (h_f) may be approximated as that at a free overfall, and this may be expressed as the coefficient of contraction (C_c) times the hydrostatic critical depth (h_c)

$$h_f = C_c \cdot h_c = C_c \cdot \left(\frac{q^2}{g}\right)^{1/3} \tag{7}$$

where q=rate of discharge per unit width of gate (Rouse 1936).

On the other hand, the resultant forces $P_i(i=1,2)$ can be estimated with the expressions

$$P_1 = \frac{\gamma \cdot H^2}{2} \tag{8a}$$

and

$$P_2 = \frac{\gamma \cdot H^2}{2}\left[1 - \left(1 - \frac{a}{H}\sin\theta_0\right)^2\right] \tag{8b}$$

corresponding to the hydrostatic pressure distributions on DD' and AA^{iv}, respectively. The approach depth (H) may be obtained from the discharge rating curve (e.g., Bradley 1954).

The flow velocities U and u may be estimated directly on the basis of continuity, given the incoming flow q, i.e.

$$u = U \cdot \left(\frac{H}{h_f}\right) = \frac{q}{h_f} \tag{9}$$

Now, the reactive force R_2 may also be computed, from Eq. (2), as

$$R_2 = (P_1 - P_2) + \frac{\gamma}{g}(U^2 \cdot H - u^2 \cdot h_f) \tag{10}$$

Fig. 5 shows the free-body diagram of the idealized gate subjected to the hydraulic forces R_1 and R_2 (per unit width of gate) and the corresponding internal reactions at the base of the cantilever, where N_0, V_0, and M_0 represent the axial load, shear force, and bending moment per unit width of gate. The equilibrium formulation leads to the following force transformation (Przemieniecki 1985):

$$\begin{Bmatrix} N_0 \\ V_0 \end{Bmatrix} = \begin{bmatrix} \cos\theta_0 & \sin\theta_0 \\ -\sin\theta_0 & \cos\theta_0 \end{bmatrix} \cdot \begin{Bmatrix} -R_1 \\ R_2 \end{Bmatrix} \tag{11a}$$

which allows the direct evaluation of the shear force

$$V_0 = R_1\sin\theta_0 + R_2\cos\theta_0 \tag{11b}$$

Eq. (11b) provides one of the boundary conditions for the boundary-value problem to be formulated next. The other boundary condition is given by the fact that the curved cantilever has a free end at B. Mathematically expressed, one has

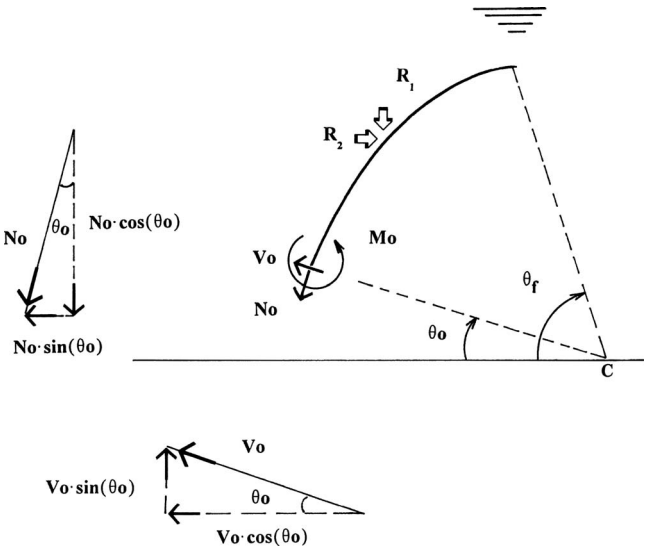

Fig. 5. Free-body diagram of gate section

$$V(\theta_0) = V_0$$
$$V(\theta_f) = 0 \tag{12}$$

Now, if the analysis leading to Eqs. (6) and (10) for the hydraulic forces is generalized for an end elevation θ, instead of θ_f [Fig. 2(b)], the following expressions are obtained:

$$R_1(\theta) = \gamma\left\{ah(\cos\theta_0 - \cos\theta) + a^2\left[\cos\theta_0(\sin\theta - \sin\theta_0) - \frac{1}{4}(\sin 2\theta - \sin 2\theta_0) - \frac{1}{2}(\theta - \theta_0)\right]\right\} \tag{13a}$$

and

$$R_2(\theta) = \frac{\gamma H^2}{2}\left[\left(1 - \frac{a}{H}\sin\theta_0\right)^2 - 2\frac{U^2}{g}\left(\frac{1}{h} - \frac{1}{H}\right)\right] \tag{13b}$$

where h=water depth of the nappe at the crest of the generalized cantilever AF. After some algebraic manipulations, the first two derivatives of each of these expressions may be obtained as

$$\frac{dR_1}{d\theta} = \gamma a^2\cos\theta\left[\left(\frac{h}{a}\right)\tan\theta + \frac{\eta^2(\cos\theta_0 - \cos\theta)}{\eta^2 - 1}\right] \tag{14a}$$

$$\frac{d^2R_1}{d\theta^2} = \gamma a^2\left\{\left(\frac{h}{a}\right)\cos\theta + \frac{\sin 2\theta}{2(\eta^2 - 1)} + \frac{\eta^2}{\eta^2 - 1}(\sin 2\theta - \sin\theta\cdot\cos\theta_0) + 3\left(\frac{a}{h}\right)\left(\frac{1 + \cos 2\theta}{2}\right)(\cos\theta_0 - \cos\theta)\frac{\eta^2}{(\eta^2 - 1)^3}\right\} \tag{14b}$$

$$\frac{dR_2}{d\theta} = \gamma ah\cos\theta\frac{\eta^2}{\eta^2 - 1} \tag{14c}$$

and

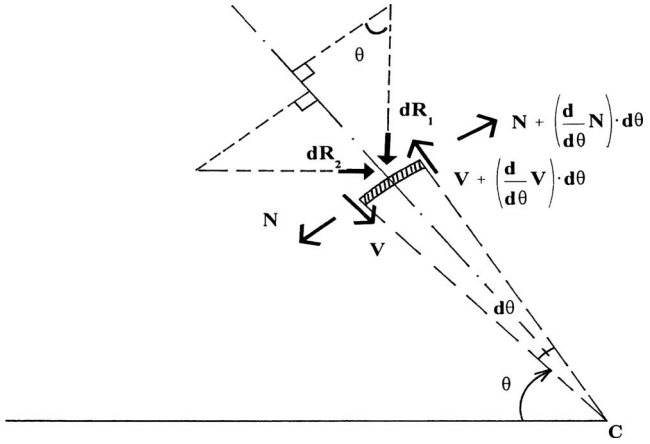

Fig. 6. Free-body diagram of gate differential element

$$\frac{d^2R_2}{d\theta^2} = \gamma a^2\left\{\frac{\eta^2}{\eta^2 - 1}\left[\frac{\cos^2\theta}{\eta^2 - 1} - \left(\frac{h}{a}\right)\sin\theta\right] + \frac{3(\eta\cos\theta)^2}{(\eta^2 - 1)^3}\right\} \tag{14d}$$

where

$$\eta^2 = \left(\frac{U^2}{gh}\right)\left(\frac{H}{h}\right)^2 \tag{14e}$$

Next, consider the free-body diagram of the differential element of gate in Fig. 6. The equilibrium of forces in the radial and tangential directions leads respectively to

$$R_1'\sin\theta + R_2'\cos\theta + N = \frac{dV}{d\theta} \tag{15a}$$

and

$$R_2'\sin\theta - R_1'\cos\theta + V + \frac{dN}{d\theta} = 0 \tag{15b}$$

where the prime symbol represents derivative with respect to θ.

Eliminating $dN/d\theta$ from Eqs. (15*a*) and (15*b*), one obtains the following governing second-order ordinary differential equation:

$$2R_1'\cos\theta - 2R_2'\sin\theta + R_1''\sin\theta + R_2''\cos\theta = V + \frac{d^2V}{d\theta^2} \tag{15c}$$

which together with the boundary conditions (12) constitute a boundary-value problem for $V(\theta)$.

This boundary-value problem is iteratively transformed into an initial-condition problem in the θ domain and subsequently solved numerically using a Fourth-Order Runge-Kutta method (Kreyszig 1988). The total pressure field is then given by (see Appendix for the derivation of a closed-form analytical expression of the hydraulic pressure field on the upstream gate skin)

$$p_t(\theta) = \frac{1}{a}\frac{dV}{d\theta} \tag{16}$$

The calculation of the torque per unit width of gate transmitted by the hydraulic pressure field to the gate tube (M_R) requires the previous evaluation of the lever arms r_1 and r_2. These lever arms are obtained from the simultaneous solution of Eqs. (3) and (4). Segment y_2, required to completely define this system of equations, may be computed from

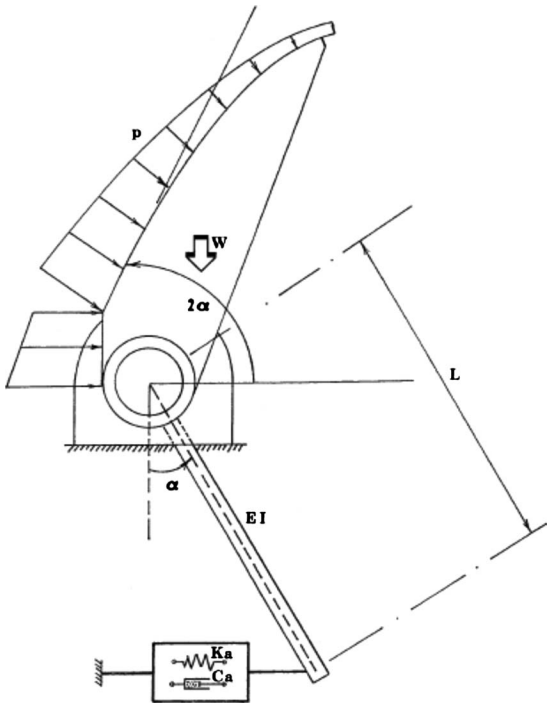

Fig. 7. Lateral view of gate components, properties, and external forces

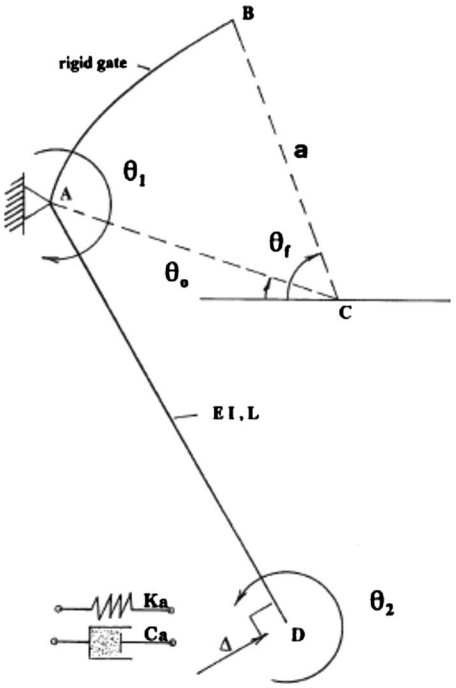

Fig. 8. Structural coordinates and single-degree-of-freedom (1-DOF) θ_1

$$y_2 = a \sin \theta_0 - \bar{y} \tag{17a}$$

where

$$\bar{y} = \frac{1}{P_2}\frac{\gamma H^3}{6}\left[1 - \left(1 - \frac{a}{H}\sin\theta_0\right)^3 - 3\left(\frac{a}{H}\right)\left(1 - \frac{a}{H}\sin\theta_0\right)^2 \sin\theta_0\right] \tag{17b}$$

Subsequently, the hydraulic torque per unit width of gate may be obtained as

$$M_R = R_1 r_1 + R_2 r_2 \tag{18}$$

Structural Response

Mean Gate Rotation

The gate system is conceived as a rigid-body torque-tube circular gate standing on simple supports and being acted upon by the hydraulic pressure field and by the viscoelastic system of resisting forces provided by the operating arms and the horizontal actuator.

Consider the rigid-body gate in closed position (elevation $=2\alpha$) shown in Fig. 7, standing on simple supports and being excited by an external dynamic pressure field p and its own weight W (mass $M=W/g$). The overturning moment of the external forces about the center of the tube is resisted by the eccentric force exerted by the horizontal actuator with stiffness K_a and equivalent viscous damping C_a, acting at the end of the operating arms with flexural rigidity EI and length L.

The analytical model for this structure is shown in Fig. 8. The gate is idealized as a rigid circular arc (radius a) spanning the elevation θ from θ_o (at A) to θ_f (at B), and its mass is lumped at the centroidal point. The torque-tube reduces to point A. The connection of the operating arms to the base of the gate at point A is rigid.

The displacements are discretized in this model by the three coordinates shown in Fig. 8, i.e., rotations θ_1 and θ_2 at Nodes A and D, respectively, and the linear displacement Δ of the end D of the operating arms. Only the strain energy associated with bending deformations of the operating arms is considered. The stiffness matrix of the system may be formulated as

$$[K] = \frac{2EI}{L}\begin{bmatrix} 2 & 1 & \frac{3}{L} \\ 1 & 2 & \frac{3}{L} \\ \frac{3}{L} & \frac{3}{L} & \left(\frac{6}{L^2} + \frac{K_a \cdot L \cdot \cos^2\alpha}{2EI}\right) \end{bmatrix} \tag{19}$$

Elimination of coordinates θ_2 and Δ from the corresponding stiffness formulation by static condensation (Przemieniecki 1985) produces the generalized stiffness coefficient for the degree of freedom θ_1 only as

$$K^* = \frac{1}{\frac{L}{3EI} + \frac{1}{K_a \cdot L^2 \cdot \cos^2\alpha}} \tag{20}$$

A similar procedure applied to the viscous damping matrix renders the generalized viscous damping coefficient associated with the degree of freedom θ_1 only as

$$C^* = C_a \cdot L^2 \cdot \cos^2\alpha + C_D^* \tag{21}$$

where C_D^*=generalized viscous damping coefficient associated with that of an equivalent viscous damper representing the energy dissipation mechanism from the structure itself plus the effect of the drag force on the gate opposing its velocity through water.

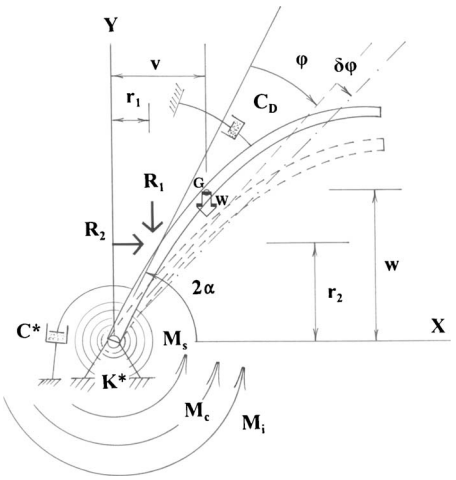

Fig. 9. Dynamic equilibrium of 1-DOF rigid-body gate system; virtual displacement

Fig. 9 shows the generalized single degree-of-freedom system ($\varphi=\theta_1$) vibrating under the action of the vertical and horizontal components of the mean hydraulic force on the gate (R_1 and R_2, respectively), the gate's own weight (W) and the resisting elastic, viscous, and inertial moments (M_s, M_c, and M_i, respectively) at the gate base. Notice in the figure the viscous damper with coefficient C_D that exerts the drag force on the gate. The degree of freedom φ is defined as the rotation of the gate with respect to its static weight-deflected configuration (Clough and Penzien 1993).

The dynamic equilibrium of the rigid-body gate is formulated by applying the virtual work principle on the structural system subjected to the virtual displacement $\delta\varphi$ (i.e., to a small variation from the instantaneous position of equilibrium defined by φ) (Mura and Koya 1992).

Ignoring negligible terms, the energy equation $\Sigma(\delta\text{Work})=0$ reduces to

$$\frac{d^2\varphi}{dt^2}+2\xi_w\omega\frac{d\varphi}{dt}+\omega^2\cdot\varphi=\frac{R_1r_1+R_2r2}{I_0}=\frac{M_0}{I_0} \tag{22a}$$

where I_0=mass moment of inertia of the gate about the tube axis

$$\omega^2=\frac{3EI}{I_0\cdot L} \tag{22b}$$

the square of the natural circular frequency of vibration; and $\xi_w=C^*/I_0$=overall equivalent viscous damping ratio of the upstream-wet gate system.

After taking expectations, the steady-state part of the solution of Eq. (22*a*) (i.e., the mean steady-state gate rotation) tends asymptotically to the limiting value (Clough and Penzien 1993)

$$\varphi_L=\frac{M_0}{\omega^2\cdot I_0} \tag{23}$$

where $M_0=E(M_R)$=mean value of M_R.

Second Moment of Hydraulic Torque on the Gate Tube

Let the hydraulic pressure field be monitored by nine pressure cells located at discrete points (strategically distributed) on the upstream face of the gate. The governing equation of motion for the gate subjected to the upstream pressure field may be written as

$$\frac{d^2v_1}{dt^2}+2\xi_w(2\pi f_1)\frac{dv_1}{dt}+(2\pi f_1)^2v_1=\left(\frac{d_1^2}{I_0}\right)\cdot\sum_{i=1}^{9}(A_i\cdot\gamma_i)p_i(t) \tag{24a}$$

where $p_i(i=1,2,\ldots,9)$=pressure acting at the ith pressure cell location, assumed as uniformly distributed over its tributary area (A_i); f_1=natural frequency of vibration of the dry gate system; $v_1=d_1\cdot\varphi$ and $\gamma_i=d_i/d_1$, with d_i=distance from the line of action of the force associated with p_i to the tube axis.

Consider the particular case when $p_i=\delta(t)$ (i.e., a Dirac delta function applied at the starting time) acts alone. Eq. (24*a*) then becomes (Bendat and Piersol 1993)

$$\frac{d^2v_{1i}}{dt^2}+2\xi_w(2\pi f_1)\frac{dv_{1i}}{dt}+(2\pi f_1)^2v_{1i}=\left(\frac{d_1^2}{I_0}\right)\cdot(A_i\gamma_i)\delta(t) \tag{24b}$$

By Fourier transforming Eq. (24*b*), one obtains the complex frequency response function between the pressure p_i and the displacement v_1 as

$$H_{1i}(f)=\frac{\frac{d_1^2}{K'}(A_i\gamma_i)}{1-\left(\frac{f}{f_1}\right)^2+i(2\xi_w)\left(\frac{f}{f_1}\right)} \tag{25}$$

where $K'=3\text{EI}/L$.

Therefore, the Fourier transform of v_1 is given by (Crandall and Mark 1963)

$$V_{1i(f)}=H_{1i(f)}\cdot P_{i(f)} \tag{26}$$

where $P_i(f)$=Fourier transform of $p_i(t)$.

The Fourier transform of the total response $v_1(t)$ is conveniently obtained by superposition in the frequency domain as

$$V_1(f)=\sum_{i=1}^{9}H_{1i}(f)\cdot P_i(f) \tag{27}$$

By taking the inverse Fourier transform of Eq. (27), the total response $v_1(t)$ in the time domain is obtained as

$$v_1(t)=\sum_{i=1}^{9}\frac{d_1^2}{K'}(A_i\gamma_i)\int_{-\infty}^{+\infty}\frac{P_i(f)e^{i2\pi ft}df}{1-\left(\frac{f}{f_1}\right)^2+i(2\xi_w)\left(\frac{f}{f_1}\right)} \tag{28}$$

The total hydraulic torque on the gate tube is given by

$$M_R(t)=K'\varphi(t)=\frac{3EI}{L}\varphi(t) \tag{29a}$$

or

$$M_R(t)=d_1\cdot\sum_{i=1}^{9}(A_i\gamma_i)\int_{-\infty}^{+\infty}\frac{P_i(f)e^{i2\pi ft}df}{1-\left(\frac{f}{f_1}\right)^2+i(2\xi_w)\left(\frac{f}{f_1}\right)} \tag{29b}$$

If the pressure p_i is assumed a zero-mean stationary (and ergodic) process (by extracting the time-average from the record), then, on the basis of linearity, the response v_{1i} and its contribution to the hydraulic torque ($M_{R,i}$)=zero-mean stationary (and ergodic) processes. Consequently, the following relations among their corresponding spectral density functions hold

$$S_{M_{R,i}}(f) = \left(\frac{K'}{d_1}\right)^2 \cdot S_{v_{1i}}(f)$$
$$= \left(\frac{K'}{d_1}\right)^2 \cdot |H_{1i}(f)|^2 \cdot S_{pi}(f)$$
$$= \left(\frac{K'}{d_1}\right)^2 \cdot \left[\frac{d_1^2}{K'}(A_i\gamma_i)\right]^2 \frac{S_{pi}(f)}{\left[1-\left(\frac{f}{f_1}\right)^2\right]^2 + \left[(2\xi_w)\left(\frac{f}{f_1}\right)\right]^2} \tag{30}$$

By adding the contribution of all p_i's to the total power, one obtains for the mean square of the hydraulic torque on the gate tube

$$E(M_R^2) = d_1^2 \cdot \sum_{i=1}^{9} (A_i\gamma_i)^2 \cdot \int_{-\infty}^{+\infty} \frac{S_{pi}(f)df}{\left[1-\left(\frac{f}{f_1}\right)^2\right]^2 + \left[(2\xi_w)\left(\frac{f}{f_1}\right)\right]^2} \tag{31a}$$

or

$$E(M_R^2) = d_1^2 \cdot \sum_{i=1}^{9} (A_i\gamma_i)^2 \cdot \int_{0}^{+\infty} \frac{G_{pi}(f)df}{\left[1-\left(\frac{f}{f_1}\right)^2\right]^2 + \left[(2\xi_w)\left(\frac{f}{f_1}\right)\right]^2} \tag{31b}$$

in terms of the half-range spectral density function $G_{pi}(f)$ (Bendat and Piersol 1993), and the corresponding variance is given by

$$\sigma_{M_R}^2 = E(M_R^2) - [E(M_R)]^2 = E(M_R^2) - M_0^2 \tag{31c}$$

Experimental Verification

It should be emphasized that multiple flow-induced loading conditions on the physical model were examined in the overall study, corresponding to diverse gate operating modes (Fletcher and de Béjar 1995). However, the theoretical models developed in this paper consider only the controlling gate-system configuration, whose geometric characteristics were idealized for mathematical tractability, in the light of the conservation principles of fluid mechanics and the theory of stationary random processes for structural dynamics. Other gate and flow configurations require different formulations, since they constitute substantially different physical problems. Among the complicating factors observed in other gate configurations are: the very influential effect of a turbulent pressure field on the downstream face of the gates, exerted by a returning tailwater jet, the vibrations induced by the entrapped air in unventilated nappes, and the edge effects at neighboring partially open gates.

Mean Pressure Field

The theoretical formulations are verified with an instrumented 1/15-scale brass model of a Montgomery Point torque-tube gate (Fig. 3). Fig. 10 shows a schematic perspective of the physical model, indicating the location of nine remotely controlled (thermally insulated) pressure cells used to monitor the hydraulic pressure field.

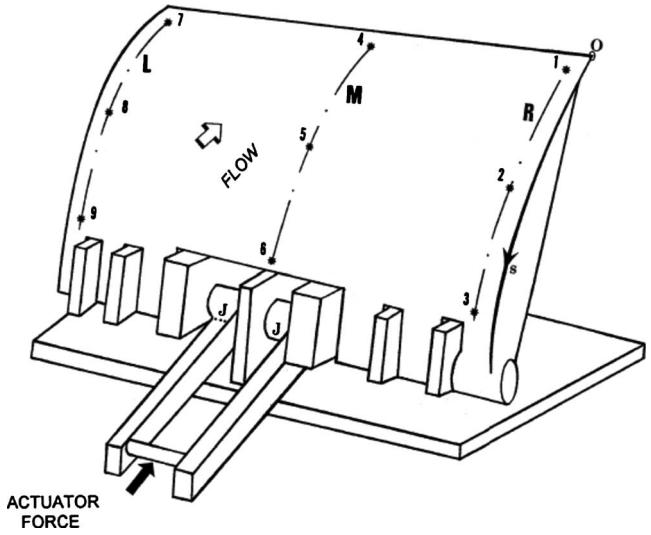

Fig. 10. Schematic perspective of gate physical model

The geometry of the gate and its operational hydraulic environment is defined by the radius $a=498$ mm, the end elevations $\theta_0=20°$ and $\theta_f=72.75°$, the depth of the incoming flow $d=628$ mm, the approach depth $H=557$ mm, and the design rate of discharge per unit width of gate $q=8\times10^4$ mm^3/(s mm). Taking the coefficient of contraction as $C_c=0.68$ [an average of several values reported in the literature (Rouse 1936)], Eq. (7) gives $h_f=59$ mm.

The mean values of the entering and exiting flow velocities may be calculated using Eq. (9) as $U=0.144$ m/s and $u=1.356$ m/s. Now, Eqs. (6) and (10) give the vertical and horizontal components of the mean force exerted by the flow on the gate as $R_1=51.28$ N and $R_2=63.54$ N, respectively, thus allowing the calculation of the boundary shear force V_0. Eq. (11*b*) gives $V_0=77.00$ N.

Given the numerical solution of Eq. (15*c*), the evaluation of Eq. (16) yields the mean pressure field, which is cast in nondimensional form by normalizing with respect to the approach hydrostatic pressure $p_n=\gamma\cdot H$. The resulting nondimensional pressure distribution (p_t/p_n) is shown graphically in Fig. 11 as a function of the normalized circumferential coordinate s/L_a on the gate arc, with origin at the gate crest and increasing downwards (normalized with respect to the total arc length, $L_a=a\cdot(\theta_f-\theta_0)=459$ mm). This figure also shows the minimum and maximum values of the experimental pressure acting on the upstream side of the 1/15-scale physical model of the gate during the controlling 100-s test. The pressure field is described along three different gate arcs: the left edge, the middle arc, and the right edge (see Fig. 10). Each of these curves represents a parabolic fit on three data points. These minimum and maximum curves delimit narrow bands, suggesting very little fluctuation of the pressure at a given location during the test. The theoretical estimation of the pressure field is an excellent upper bound over most of the domain for the gate central arc, except on a small region in the middle third, where the estimation is slightly unconservative. Imperfect sealing at the edges of the instrumented gate (the central gate in the set of 3) allows the formation of lateral jetting, which induces an observed increase in pressure on the upper corners of the gate, as compared with the theoretical prediction (left and right edges in Fig. 11).

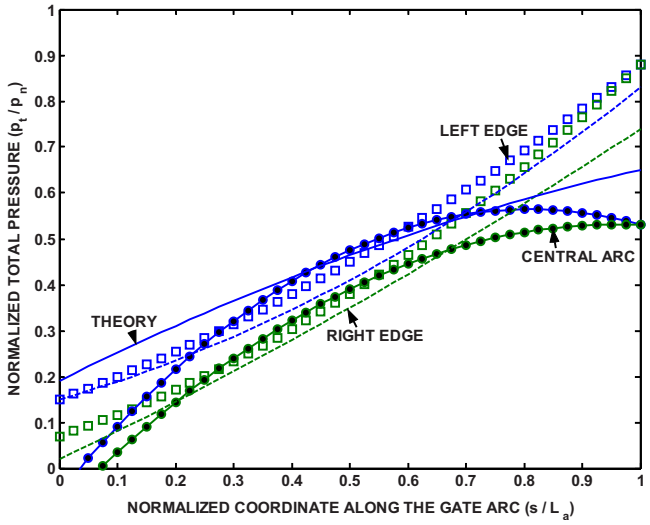

Fig. 11. Comparison of theoretical prediction of hydraulic pressure field with corresponding experimental pressure range

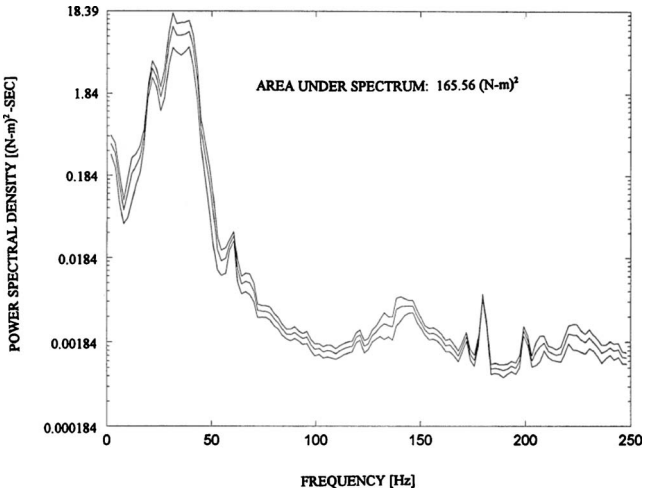

Fig. 13. Spectral density of bending moment at cross sections J of operating arms, i.e., at the joint with gate tube

Mean Torque on the Gate Tube

The numerical solution of Eqs. (3) and (4) and the subsequent evaluation of Eq. (18) yield the mean hydraulic torque on the gate tube as $M_0=117.2$ N m/m. This theoretical estimation differs from the average experimental hydraulic torque during ventilated-nappe tests (105.7 N m/m) by 11%, on the conservative side. The discrepancy between the theoretical prediction and the experimental value is due in part to the fact that the quantity experimentally measured is the bending moment at the end of the operating arms (sections J in Fig. 10), which differs somewhat from the hydraulic torque on the gate tube. The agreement between theory and experiments is generally good.

Mean Gate Rotation

Fig. 12 shows a relevant portion of the free-vibration decay of the physical model with water on its upstream side only, and the application of the logarithmic decrement method to identify the equivalent viscous damping ratio: $\xi_w=9.5\%$, on the average (Clough and Penzien 1993).

If Young's modulus of elasticity for brass is taken as $E=106.9\times10^3$ MPa, the moment of inertia of both operating

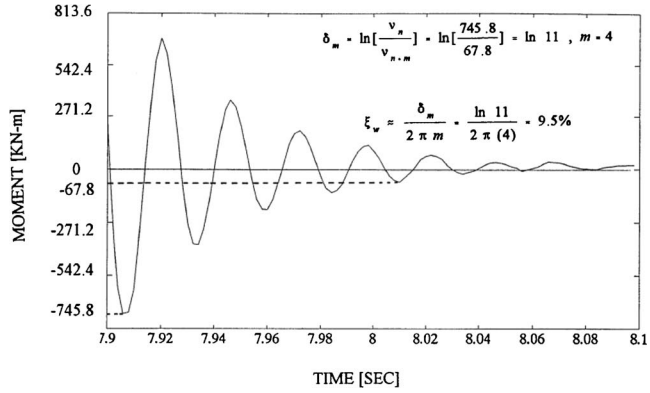

Fig. 12. Identification of equivalent viscous damping ratio of gate with submerged upstream side

arms about their neutral axis in bending is calculated as $I=9.25\times10^4$ mm^4, and it is recognized that $L=236$ mm, then Eqs. (22*b*) and (23) give $\varphi_L=0.0315$. Experimental measurements on the physical model with a ventilated nappe subjected to carefully controlled hydraulic pools gave $\varphi_L=0.0350°$, on the average. Therefore, the theoretical prediction is generally in good agreement with the experimental observations.

Mean Square Torque on the Gate Tube

Eq. (29*b*) is evaluated numerically using the pressure-cell records. For example, using the controlling test with a duration of 100 s and data obtained at a rate of 500 samples/s, the value of the power adds up to $E(M_R^2)=4,054$ (N m)^2, which is compared to the experimental value

$$E(M_R^2)=\sigma_{M_R}^2+\mu_{M_R}^2=165.00+69.17^2=4949 \text{ (N m)}^2$$

where $\sigma_{M_R}^2$=variance of the random process M_R, given by the area under the corresponding spectral density function (Fig. 13), and μ_{M_R} is the mean of the process. Again, the mean square of the directly measured process $E(M_R^2)$ differs from its value derived from the hydraulic pressure field partly because the directly measured process is the bending moment at the end of the operating arms. However, results compare generally well (~18% relative difference, on the unconservative side).

Conclusions

The upstream pressure field on a typical navigable spillway torque-tube gate is constructed analytically. The critical hydrostructural configuration is considered, i.e., the upstream flow at its maximum operational headwater pool running over a set of torque-tube gates in a fully closed position. Experimental observations indicate that this critical condition is conservatively simplified in the theoretical model by neglecting the effect of the tailwater pressure. The mean steady-state rotation response of the gate is formulated, and the second-moment characterization of the torque transmitted to the gate tube is presented.

The mean pressure field gives an excellent upper bound over most of the domain for the central region of the gate skin. On

the gate corners, however, the theory underestimates the observations. At least in part, this underestimation is due to edge effects in the subscale physical model. Derived mean values of parameters of response are sufficiently close to the experimental observations (on the average, 11% overprediction for the hydraulic torque induced in the gate tube) and may be used in the preliminary design of a gate for the application being considered.

The dispersion of parameters of response is needed for the final design of a gate. These statistics are directly related to the corresponding mean square quantities. In this study, the mean square value of the parameter under consideration is obtained empirically (e.g., using physical modeling). The mean square value of the hydraulic torque induced in the gate tube is underpredicted (on the average, with 18% error) when derived from pressure records, as compared to the corresponding mean square value measured directly. The simplifying assumptions in the structural model and measurement errors are the major contributors to this discrepancy. In practice, however, having only the pressure records, the analyst may derive straightforwardly the dispersion of any other parameter of interest without having to measure it directly.

The agreement between theory and experiments is remarkable, given the errors associated with the simplifying assumptions under the theory, and the design of the physical model and its actual construction, assemblage, and installation.

The physical subscale replica of the scenario for the torque-tube gate in service constitutes an imperfect Froude's model that allows the estimation of the basic design hydrodynamic forces on the prototype gate on the basis of similarity principles (Fletcher and de Béjar 1995). Although some scale effects are ignored (like the added-mass effects in the hydrodynamic response of the prototype, for example), the results provide invaluable quantitative guidance to the designer that would be difficult to estimate without the experimental observations and the subsequent analysis conducted in this investigation.

Acknowledgments

This investigation was conducted at the U.S. Army Engineer Research and Development Center through the Montgomery Point Lock and Dam Gate Study, sponsored by Headquarters, U.S. Army Corps of Engineers at the request of the U.S. Army Engineer District, Little Rock. The writers gratefully acknowledge permission from the authorities at the U.S. Army Engineer District, Little Rock, and from the Chief of Engineers to publish the information in this paper.

Appendix. Hydraulic Pressure Field on the Upstream Gate Skin in Closed Form

Governing differential Eq. (15*c*) for the shear force function $V(\theta)$ is given by

$$V'' + V = (2 \cdot R_1' + R_2'') \cdot c\theta - (2 \cdot R_2' - R_1'') \cdot s\theta \tag{32}$$

in which $c\theta = \cos(\theta)$ and $s\theta = \sin(\theta)$. Inserting Eqs. (14*a*)–(14*d*) into Eq. (32) renders

$$V'' + V = \gamma a^2 \cdot k \cdot \left\{ -\frac{3}{2} \cdot \frac{h}{a} \cdot \frac{1}{\eta^2} \cdot s2\theta + \frac{k^2 c\theta}{\eta^2} \times \left(1 + \frac{1}{2\eta^4} - \left[2 \cdot (\eta^2 - 2) + \frac{1}{2\eta^4} \right] \cdot c2\theta \right) + \frac{c\theta_0}{2} \cdot (1 + 3 \cdot c2\theta) + \frac{3k^2}{\eta^4 \cdot \frac{h}{a}} \cdot s\theta \cdot (c\theta_0 - c\theta) \cdot c^2\theta \right\} \tag{33}$$

in which $k = 1/(1 - 1/\eta^2)$. The general solution of Eq. (33) is obtained as

$$V(\theta) = A \cdot c\theta + B \cdot s\theta + V_p(\theta) \tag{34a}$$

where the particular solution is given by

$$V_p(\theta) = \frac{\gamma a^2 \cdot k}{2} \cdot \left\{ c\theta_0 + \frac{k^2 \cdot \theta}{\eta^2} \cdot \left[\left(3 - \eta^2 + \frac{1}{4\eta^2} \right) \cdot s\theta - \frac{3}{4} \cdot \frac{c\theta_0}{\eta^2 \cdot \frac{h}{a}} \cdot c\theta \right] + \frac{1}{\eta^2} \cdot \left(\frac{h}{a} + \frac{k^2}{2\eta^2 \cdot \frac{h}{a}} \right) \cdot s2\theta - c\theta_0 \cdot c2\theta - \frac{3}{16} \cdot \frac{k^2 \cdot c\theta_0}{\eta^4 \cdot \frac{h}{a}} \cdot s3\theta + \frac{k^2}{4\eta^2} \cdot \left(\eta^2 - 2 + \frac{1}{4\eta^4} \right) \cdot c3\theta + \frac{k^2}{20\eta^4 \cdot \frac{h}{a}} \cdot s4\theta \right\} \tag{34b}$$

Upon imposing the boundary conditions stipulated by Eqs. (12), the set of constants $\{A, B\}$ in the complementary solution to Eq. (33) is obtained as

$$\begin{Bmatrix} A \\ B \end{Bmatrix} = \frac{1}{\sin(\theta_f - \theta_0)} \cdot \begin{Bmatrix} [V_0 - V_p(\theta_0)] \cdot s\theta_f + V_p(\theta_f) \cdot s\theta_0 \\ -[V_0 - V_p(\theta_0)] \cdot c\theta_f - V_p(\theta_f) \cdot c\theta_0 \end{Bmatrix} \tag{35}$$

Thereafter, Eq. (16) provides an analytical expression in closed form for the total hydraulic pressure field on the upstream gate skin

$$p_t(\theta) = \frac{1}{a}\frac{dV(\theta)}{d\theta} = \frac{1}{a}(-A \cdot s\theta + B \cdot c\theta) + \frac{\gamma a \cdot k}{2} \cdot \left\{ 2c\theta_0 \cdot s2\theta + \frac{k^2}{\eta^2} \cdot \left[\left(3 - \eta^2 + \frac{1}{4\eta^2} \right) \cdot (\theta \cdot c\theta + s\theta) + \frac{3}{4}\frac{c\theta_0}{\eta^2 \cdot \frac{h}{a}} \cdot (\theta \cdot s\theta - c\theta) + 2 \cdot \left(\frac{1}{k^2} \cdot \frac{h}{a} + \frac{1}{2\eta^2 \cdot \frac{h}{a}} \right) \cdot c2\theta - \frac{9}{16} \cdot \frac{c\theta_0}{\eta^2 \cdot \frac{h}{a}} c3\theta - \frac{3}{4} \cdot \left(\eta^2 - 2 + \frac{1}{4\eta^4} \right) \cdot s3\theta + \frac{1}{5} \cdot \frac{1}{\eta^2 \cdot \frac{h}{a}} \cdot c4\theta \right] \right\} \tag{36}$$

When the approach velocity U is very large ($U \to \infty$), Eq. (33) for the shear force function $V(\theta)$ reduces to

$$V'' + V = -\gamma a^2 \cdot \left\{ -\frac{c\theta_0}{2} + c\theta - \frac{3}{2} \cdot c\theta_0 \cdot c2\theta + c3\theta \right\} \quad (37)$$

with the general solution

$$V_\infty(\theta) = A_\infty \cdot c\theta + \left(B_\infty - \frac{\gamma a^2}{2} \cdot \theta \right) \cdot s\theta + \gamma a^2 \cdot \left(c\theta_0 \cdot s^2\theta + \frac{1}{8} \cdot c3\theta \right) \quad (38)$$

Upon imposing the boundary conditions stipulated by Eqs. (12), the set of constants $\{A_\infty, B_\infty\}$ in the complementary solution to Eq. (37) is obtained as

$$\begin{Bmatrix} A_\infty \\ B_\infty \end{Bmatrix} = \frac{1}{\sin(\theta_f - \theta_0)} \cdot \begin{Bmatrix} V_0 \cdot s\theta_f - \frac{\gamma a^2}{2} \cdot \left[s\theta_0 \cdot s\theta_f \cdot (\theta_f - \theta_0 - 2c\theta_0 \cdot (s\theta_f - s\theta_0)) + \frac{1}{4}(s\theta_f \cdot c3\theta_0 - s\theta_0 \cdot c3\theta_f) \right] \\ -V_0 \cdot c\theta_f - \frac{\gamma a^2}{2} \cdot \left[c\theta_0 \cdot s\theta_f \cdot (2s\theta_f \cdot c\theta_0 - \theta_f) - c\theta_f \cdot s\theta_0 \cdot (s2\theta_0 - \theta_0) + \frac{1}{4}(c\theta_0 \cdot c3\theta_f - c\theta_f \cdot c3\theta_0) \right] \end{Bmatrix} \quad (39)$$

Thereafter, Eq. (16) provides an analytical expression in closed form for the total hydraulic pressure field on the upstream gate skin, as $U \to \infty$

$$p_{t\infty}(\theta) = \frac{1}{a}\frac{dV_\infty(\theta)}{d\theta} = \frac{1}{a}(-A_\infty \cdot s\theta + B_\infty \cdot c\theta) + \frac{\gamma a}{2} \cdot \left(-\theta \cdot c\theta - s\theta + 2c\theta_0 \cdot s2\theta - \frac{3}{4} \cdot s3\theta \right) \quad (40)$$

Similarly, when the approach velocity U is very small ($U \to 0$), Eq. (33) for the shear force function $V(\theta)$ reduces to

$$V'' + V = \frac{\gamma a^2}{2} \cdot \left\{ 3\frac{h}{a} \cdot s2\theta - \frac{1}{2}c\theta + \frac{1}{2}c3\theta \right\} \quad (41)$$

with the general solution

$$V_o(\theta) = A_o \cdot c\theta + B_o \cdot s\theta - \frac{\gamma a^2}{8} \cdot \left(\theta \cdot s\theta + 4\frac{h}{a} \cdot s2\theta + \frac{1}{4} \cdot c3\theta \right) \quad (42)$$

Upon imposing the boundary conditions stipulated by Eqs. (12), the set of constants $\{A_o, B_o\}$ in the complementary solution to Eq. (41) is obtained as

$$\begin{Bmatrix} A_o \\ B_o \end{Bmatrix} = \frac{1}{\sin(\theta_f - \theta_0)} \cdot \begin{Bmatrix} V_0 \cdot s\theta_f + \frac{\gamma a^2}{8} \cdot \left[s\theta_f \cdot \left(\theta_0 \cdot s\theta_0 + 4\frac{h}{a} \cdot s2\theta_0 + \frac{1}{4} \cdot c3\theta_0 \right) - s\theta_0 \cdot \left(\theta_f \cdot s\theta_f + 4\frac{h}{a} \cdot s2\theta_f + \frac{1}{4} \cdot c3\theta_f \right) \right] \\ -V_0 \cdot c\theta_f + \frac{\gamma a^2}{8} \cdot \left[-c\theta_f \cdot \left(\theta_0 \cdot s\theta_0 + 4\frac{h}{a} \cdot s2\theta_0 + \frac{1}{4} \cdot c3\theta_0 \right) + c\theta_0 \cdot \left(\theta_f \cdot s\theta_f + 4\frac{h}{a} \cdot s2\theta_f + \frac{1}{4} \cdot c3\theta_f \right) \right] \end{Bmatrix} \quad (43)$$

Thereafter, Eq. (16) provides an analytical expression in closed form for the total hydraulic pressure field on the upstream gate skin, as $U \to 0$

$$p_{to}(\theta) = \frac{1}{a}\frac{dVo(\theta)}{d\theta} = \frac{1}{a}(-A_o \cdot s\theta + B_o \cdot c\theta) - \frac{\gamma a^2}{8} \cdot \left(\theta \cdot c\theta + s\theta + 8\frac{h}{a} \cdot c2\theta - \frac{3}{4} \cdot s3\theta \right) \quad (44)$$

Notation

The following symbols are used in this paper:

A_i = tributary area for the ith pressure-cell location;
A_s = auxiliary area (shaded in Fig. 4);
A_B, A_D = cross sectional areas of control volume at Locations B and D, respectively;
A, A', A'', A''', A^{IV} = demarcating points in longitudinal section of control volume;
$\{A, B\}$ = set of two integration constants;
$\{A_0, B_0\}$ = set of two integration constants when approach velocity is very small;
$\{A_\infty, B_\infty\}$ = set of two integration constants when approach velocity is very large;
a = gate radius;
B, B' = demarcating points in the longitudinal section of control volume;
C = center of gate-skin circular arc;
C_D = equivalent viscous damping coefficient for drag force on gate;
C_a = equivalent viscous damping coefficient for horizontal actuator;
C_c = coefficient of contraction;
C^* = generalized overall viscous damping coefficient for a single-degree-of-freedom model;
C_D^* = generalized viscous damping coefficient for internal energy dissipation mechanism of gate structure combined with effect of drag force;

$cn\theta$ = $\cos(n\cdot\theta)$, $n=1,\ldots,4$;
D, D' = demarcating points in longitudinal section of control volume;
d = differential operator;
d_i = distance from line of action of resultant force for pressure p_i on gate skin to tube axis ($i=1,\ldots,9$);
E = Young's modulus of elasticity for brass;
$E(\ )$ = mathematical expectation operator;
e = base of natural logarithms;
F = general point on gate-skin circular arc;
f = frequency;
f_1 = natural frequency of vibration of dry-gate system (Hz);
G = gate center of gravity;
$G_{pi}(f)$ = half-range spectral density function for pressure $p_i, i=1,\ldots,9$;
g = acceleration of gravity;
H = upstream head at entrance to the control volume;
$H_{1i}(f)$ = complex frequency response function between pressure p_i and displacement v_1;
h = water depth of nappe at crest of a sectional cantilever of gate;
h_c = hydrostatic critical depth;
h_f = brink depth;
I = cross-sectional moment of inertia of operating arms about a horizontal neutral axis through their centroids;
I_o = mass moment of inertia of gate about tube axis;
i = imaginary unit $[\sqrt{(-1)}]$;
J = end sections of operating arms adjacent to torque tube;
K' = defined variable for $3EI/L$;
$[K]$ = system stiffness matrix;
K_a = axial stiffness of horizontal actuator;
K^* = generalized stiffness coefficient for a single-degree-of-freedom model;
k = defined variable for $1/(1-1/\eta^2)$;
L = label for a circular arc on gate skin parallel to left edge of gate and close to it, looking in downstream direction;
L = length of gate operating arms;
L_a = length of a circular arc at intersection of gate skin with a vertical plane, from gate crest to tube axis, at gate base;
M = label for a central circular arc on gate skin, midway between arcs **L** and **R** and parallel to them, looking in the downstream direction;
M_R = resultant hydraulic torque exerted on gate tube;
M_c = resisting viscous moment at gate base;
M_i = resisting inertial moment at gate base;
M_s = resisting elastic moment at gate base;
M_0 = equilibrating internal bending moment on gate at elevation θ_0;
m, n = subscripts indicating that m or n cycles of vibration have elapsed, respectively;
N or $N(\theta)$ = internal axial force on a gate general cross section at elevation θ;
N_0 = equilibrating internal axial force on gate, at elevation θ_0;
P_1, P_2 = resultant forces of pressures on sides DD' and AA^{IV} of control volume, respectively;
p_{at} = atmospheric pressure;
p_b = distributed vertical reaction at base of the control volume;
p_i = pressure acting at ith pressure-cell location on gate skin ($i=1,\ldots,9$);
p_n = $\gamma\cdot H$ approach hydrostatic pressure;
$p_t(\theta)$ = total hydrostatic pressure field acting on upstream gate skin at general elevation θ;
$p_{t0}(\theta)$, and $p_{t\infty}(\theta)$ = total hydrostatic pressure field acting on the upstream gate skin at general elevation θ, when approach velocity U is very small, and very large, respectively;
Q = point of application of resultant force exerted by gate on flow;
q = rate of discharge per unit width of gate;
R = label for a circular arc on gate skin parallel to right edge of gate and close to it, looking in downstream direction;
R_1, R_2 = vertical and horizontal components, respectively, of force exerted by gate on flow;
r_1, r_2 = lever arms of forces R_1 and R_2, respectively, when evaluating their moments about tube axis;
S = power spectral density function;
s = circumferential coordinate on a vertical plane and along gate skin, with origin at gate crest, and increasing downward;
$sn\theta$ = $\sin(n\cdot\theta)$, $n=1,\ldots,4$;
t = time;
U = velocity of flow entering control volume, assumed horizontal and uniform;
u = velocity of flow leaving control volume, assumed horizontal and uniform;
V or $V(\theta)$ = internal shear force on a gate general cross section at elevation θ;
$V_p(\theta)$ = particular component of general solution $V(\theta)$;
V_0 = equilibrating internal shear force on gate, at elevation θ_0;
$V_0(\theta), V_\infty(\theta)$ = general solution for $V(\theta)$ when approach velocity U is very small, and very large, respectively;
v = abscissa of center of gravity of a displaced gate;
v_1 = defined variable for $d_1\cdot\varphi$;
W = gate weight;
W_i = weight of water in the ith component of idealized control volume ($i=1,2,3$);
w = ordinate of center of gravity of a displaced gate;
X, Y = Cartesian axes of reference;
x_3 = lever arm of weight W_3 in calculating its moment about tube axis;
$\bar{x}$ = centroidal abscissa of auxiliary area;
$\bar{y}$ and y_2 = vertical distance of line of action of force P_2 from base of control volume and from tube axis, respectively;
α = angle that gate operating arms make with vertical;
γ = unit weight of water;

γ_i = defined as distance ratio d_i/d_1 $(i=1,\ldots,9)$;
Δ = displacement coordinate of end D of gate operating arms;
δ = variation operator;
δ_m = logarithmic decrement after m cycles of free oscillations;
$\delta(t)$ = Dirac delta function at time zero;
ϵ = symbol to denote "belonging to a certain set;"
η = defined variable for $(U\cdot H/h)/\sqrt{(g\cdot h)}$;
θ = angular elevation of a gate general cross section;
θ_f and θ_0 = angular elevations of gate crest and tube axis, respectively;
θ_1 and θ_2 = rotational coordinates at Ends A and D of gate operating arms, respectively;
μ = symbol for mean of a random variable;
ν_n and ν_{n+m} = amplitude of moment after n and $n+m$ cycles of free oscillations, respectively;
ξ_w = overall equivalent viscous damping ratio of upstream-wet gate system;
ρ = mass density of water;
Σ = symbol for summation operator;
σ^2 = symbol for variance of a random variable;
ω = natural circular frequency of vibration; and
φ and φ_L = gate rotation and its limit value, respectively.

References

Bendat, J. S., and Piersol, A. G. (1993). *Engineering applications of correlation and spectral analysis*, 2nd Ed., Wiley, New York.

Bradley, J. N. (1954). "Rating curves for flow over drum gates." *Trans. Am. Soc. Civ. Eng.*, 119, 403–420.

Clough, R. W., and Penzien, J. (1993). *Dynamics of structures*, 2nd Ed., McGraw-Hill, New York.

Crandall, S. H., and Mark, W. D. (1963). *Random vibration in mechanical systems*, Academic, New York.

de Béjar, L. A. (1995). "Montgomery Point Lock and Dam study: Report 2. Montgomery point torque-tube gate—A structural model study." *Technical Rep. SL-95-14*, U.S. Army Engineer Waterways Experiment Station, Vicksburg, Miss.

Fletcher, B. P., and de Béjar, L. A. (1995). "Montgomery Point Lock and Dam study: Report 1. Hydraulic forces and characteristics acting on spillway gates." *Technical Rep. SL-95-14*, U.S. Army Engineer Waterways Experiment Station, Vicksburg, Miss.

Kreyszig, E. (1988). *Advanced engineering mathematics*, 6th Ed., John Wiley and Sons, New York.

Mura, T., and Koya, T. (1992). *Variational methods in mechanics*, Oxford University Press, New York.

Naudascher, E. (1991). *Hydrodynamic forces*, Balkema, Rotterdam, The Netherlands.

Naudascher, E., and Rockwell, D. (1994). *Flow-induced vibrations: An engineering guide*, Balkema, Rotterdam, The Netherlands.

Prandtl, L., and Tietjens, O. J. (1957). *Fundamentals of hydro- and aeromechanics*, Dover Publications, Mineola, N.Y.

Przemieniecki, J. S. (1985). *Theory of matrix structural analysis*, Dover Publications, Mineola, N.Y.

Rouse, H. (1936). "Discharge characteristics of the free overfall." *Civil Engineering, ASCE*, 6(4), 257–260.

Sagar, B. T. A. (1995). "ASCE Hydrogates task committee design guidelines for high-head gates." *J. Hydr. Engrg.*, 121(12), 845–852.

Sehgal, C. K. (1996). "Design guidelines for spillway gates." *J. Hydr. Engrg.*, 122(3), 155–165.

Sehgal, C. K., Morgan, M. J., Winters, L., and Eggburn, M. (1997). "Montgomery Point Lock and Dam navigable pass gate equipment." *Proc., Int. Conf. on Hydropower*, ASCE, Atlanta, Ga., 1016–1028.

Shames, I. H. (1995). *Mechanics of fluids*, 3rd Ed., McGraw-Hill, New York.

Street, R., Watters, G. Z., and Vennard, J. (1996). *Elementary fluid mechanics*, 7th Ed., John Wiley and Sons, New York.

Viparro, V. J., and Hansen, H. (1993). *Davis' handbook of applied hydraulics*, 4th Ed., McGraw-Hill, New York.